

Development of an Autonomous Sanding Robot with Structured-Light Technology

Yingxin Huo, Diancheng Chen, Xiang Li, Peng Li, and Yun-Hui Liu

Abstract—Large demand for robotics and automation has been reflected in the sanding works, as current manual operations are labor-intensive, without consistent quality, and also subject to safety and health issues. While several machines have been developed to automate one or two steps in the sanding works, the autonomous capability of existing solutions is relatively low, and the human assistance or supervision is still heavily required in the calibration of target objects or the planning of robot motion and tasks. This paper presents the development of an autonomous sanding robot, which is able to perform the sanding works on an unknown object automatically, without any prior calibration or human intervention. The developed robot works as follows. First, the target object is scanned then modeled with the structured-light camera. Second, the robot motion is planned to cover all the surfaces of the object with an optimized transition sequence. Third, the robot is controlled to perform the sanding on the object under the desired impedance model. A prototype of the sanding robot is fabricated and its performance is validated in the task of sanding a batch of wooden boxes. With sufficient degrees of freedom (DOFs) and the module design for the end effector, the developed robot is able to provide a general solution to the autonomous sanding on many other different objects.

I. INTRODUCTION

Sanding is a common operation in the manufacturing industry, where workers stand next to a spinning sanding belt or use a portable tool to remove the coating from a target object (see Fig. 1). Current sanding operations are mainly performed by human workers, and disadvantages include: i) the labor-intensive nature, ii) the inconsistency in quality, iii) the unhealthy working environment (e.g., dust, noise) and safety issues (e.g., fatigue, injury). Therefore, the manual sanding is now with the serious problems about the shortage of skilled workers and their rapidly increasing wages.

To address the problems associated with the manual sanding. Some industry polishing machine for a specific application was developed since 2000 [1]-[3] by Nagata. In the beginning, the polishing work relied on calibration before the process, then with the CAD model of the sanded objects, the sanding trajectory could be given out according to the CAD model, but still, CAD model should be set

This work was supported by the CUHK T Stone Robotics Institute and the Innovation and Technology Commission of Hong Kong under Grant no.UIM/335 and in part by the VC Fund 4930745 of the CUHK T Stone Robotics Institute.(Corresponding author: Xiang Li (xiangli@cuhk.edu.hk), Co-corresponding author: Peng Li (peng.li@hit.edu.cn))

Y. Huo, D. Chen, X. Li and Y.-H. Liu are with the Department of Mechanical and Automation Engineering, The Chinese University of Hong Kong, Hong Kong S.A.R. X. Li is also with the CUHK Shenzhen Research Institute (SZRI), China.

P. Li is with the CUHK SZRI and the Department of Mechanical and Engineering and Automation, Harbin Institute of Technology (Shenzhen).

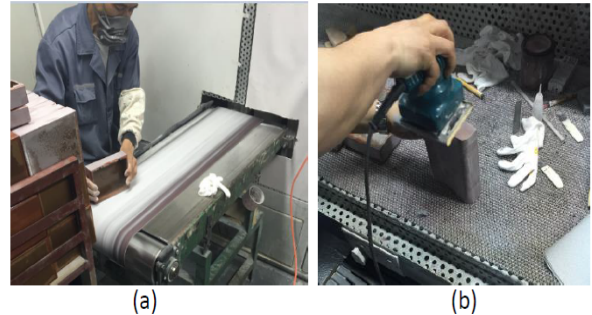


Fig. 1. Manual sanding operations (a) Sanding the wooden box on a sand paper machine (b) Sanding the wooden box with a portable tool

and the path should be calculated in advanced. With the research into control theory, in [2] feedforward controller based on the superior calculated trajectory was proposed. It was the first time the controller was adopted in generating the trajectory though it was based on the calibration data collected before the experiment. In [3] automatic polishing system was presented, the polishing path was generated through file reading or robot teaching and then drew the polishing path on the mold surface, the force controllable robot was used to polish the face. After trying the particular shape model, free-formed surface model was considered [4], but the CAD model of the sanded object was necessary and the method could only be used for one curved plane. In all these applications, human assists [1]-[5] were indispensable, even if with the CAD/CAM system, the system could only generate the sanding trajectory for one flat or curved plane based on the data collected in advanced.

As the robot is controlled to interact with the target surfaces of the sanded object, the interaction force should be regulated to guarantee the quality of sanding. There were several control methods proposed to solve the problem of interaction force and position control in the past two to three decades. Before automating the process of sanding, the automatic process using impedance controller, such as deburring, which is less stress on the compliant interaction force was proposed [6][7]. In sanding and polishing operations, there are three classes of the method to cope with the interaction force between the sanding end effector and the surface. When there is no force sensor available, the reaction force observer (RFOB) could be designed into the PD control loop to estimate the force [8]. The second method is to try to decouple the force and position control with controller design and mechanical design [9-11]. The third method is to use the impedance model to build up the impedance controller [12]. Impedance controller [12][13] was adopted to control the interaction force in many traditional and modern industry

robots and adaptive control are effective according to recent research in controller design [14]. In our application, because of the interaction force is applied at the end point of the robot, the force sensor is available, position and force control are coupled, so the adaptive impedance controller is adopted under the task space [15].

However, the autonomous capability of existing systems for automatic sanding is relatively low, in the sense that a lot of human involvement or assistance is still required in some specific steps of sanding. For example, the manual calibration is usually required to obtain the CAD model of sanded objects beforehand, or humans should specify the sequence of sanding on different surfaces of the object, or the desired trajectory of the robot should be manually set according to the human's experience, or the sanding quality is assessed by humans.

In this paper, a new autonomous sanding robot is proposed with the structured-light technology, which is to automate the labor-intensive works and hence systematically address the problems associated with manual operations. Compared with existing systems, the autonomous capability of the proposed robot is significantly improved in terms of the following aspects. First, the structured-light scanner is employed to scan the unknown object and construct its model with point clouds. Second, the model-based planner is proposed to specify the reference motion of the end effector such that it covers all the surfaces of the object under an optimized sequence. Third, the adaptive impedance controller is developed to achieve the desired impedance model and hence drive the robot to carry out the sanding task. Fourth, the quality evaluation is performed by assessing the changes of three-dimensional information of the sanded surface. Note that no human assistance or supervision is required in the above steps or the transition between steps. The stability of the closed-loop system is rigorously analyzed with Lyapunov methods, such that the proposed adaptive impedance controller is theoretically grounded. A prototype of the proposed robot is fabricated and its performance is validated in the task of sanding a batch of wooden boxes.

II. BACKGROUND

A. Robot Kinematics and Dynamics

The forward kinematic model of a robot manipulator can be given as

$$\mathbf{x} = \mathbf{h}(\mathbf{q}), \quad (1)$$

where $\mathbf{x} \in \mathfrak{R}^m$ represents the position of the robot end effector in task space (e.g. Cartesian space or vision space), $\mathbf{q} \in \mathfrak{R}^n$ is the vector of robot joint angles, and $\mathbf{h}(\cdot)$ denote the nonlinear functions. Then, the velocity of the robot end effector in task space is related to the joint-space velocity of the robot as

$$\dot{\mathbf{x}} = \mathbf{J}(\mathbf{q})\dot{\mathbf{q}}, \quad (2)$$

where $\mathbf{J}(\mathbf{q}) \in \mathfrak{R}^{m \times n}$ is the Jacobian matrix from joint space to task space.

The dynamic model of a robot manipulator can be described as

$$\mathbf{M}(\mathbf{q})\ddot{\mathbf{q}} + \mathbf{C}(\mathbf{q}, \dot{\mathbf{q}})\dot{\mathbf{q}} + \mathbf{g}(\mathbf{q}) = \mathbf{u} + \boldsymbol{\tau}_e, \quad (3)$$

where $\mathbf{M}(\mathbf{q})\ddot{\mathbf{q}} \in \mathfrak{R}^n$, $\mathbf{C}(\mathbf{q}, \dot{\mathbf{q}})\dot{\mathbf{q}} \in \mathfrak{R}^n$, and $\mathbf{g}(\mathbf{q}) \in \mathfrak{R}^n$ denote the inertia torque, the centripetal and coriolis torque, and the gravitational torque of the robot respectively, \mathbf{u} denotes the control input torque, and $\boldsymbol{\tau}_e$ denotes the interaction torque. Note that $\boldsymbol{\tau}_e = \mathbf{J}^T(\mathbf{q})\mathbf{f}_e$, and $\mathbf{f}_e \in \mathfrak{R}^m$ is the interaction force between the robot end effector and the environment.

Some important properties of the dynamic model (3) are listed as follows.

- (i) The dynamic parameters $\mathbf{M}(\mathbf{q})$, $\mathbf{C}(\mathbf{q}, \dot{\mathbf{q}})$ and $\mathbf{g}(\mathbf{q})$ are bounded;
- (ii) The matrix $\mathbf{M}(\mathbf{q})$ is symmetric and positive definite;
- (iii) The matrix $\dot{\mathbf{M}}(\mathbf{q}) - 2\mathbf{C}(\mathbf{q}, \dot{\mathbf{q}})$ is skew-symmetric.

In this paper, the dynamic parameters, i.e. $\mathbf{M}(\cdot)$, $\mathbf{C}(\cdot)$, and $\mathbf{g}(\cdot)$ are assumed to be unknown and will be estimated by on-line adaptation laws.

B. Impedance Control

In impedance control, the control objective is specified as a desired impedance model in task space as

$$\mathbf{M}_d(\ddot{\mathbf{x}} - \ddot{\mathbf{x}}_d) + \mathbf{C}_d(\dot{\mathbf{x}} - \dot{\mathbf{x}}_d) + \mathbf{K}_d(\mathbf{x} - \mathbf{x}_d) = \mathbf{f}_e - \mathbf{f}_d, \quad (4)$$

where $\mathbf{x}_d \in \mathfrak{R}^m$ denotes the time-varying desired trajectory in task space, $\mathbf{f}_d \in \mathfrak{R}^m$ is the desired force, $\mathbf{M}_d, \mathbf{C}_d, \mathbf{K}_d \in \mathfrak{R}^{m \times m}$ denote the desired inertia, the desired damping, and the desired stiffness matrices respectively, which are diagonal and constant. The desired impedance model (4) describes a dynamic relationship between the position error and the interaction force.

The desired impedance model (4) can be rewritten as

$$\Delta\ddot{\mathbf{x}} + \mathbf{M}_d^{-1}\mathbf{C}_d\Delta\dot{\mathbf{x}} + \mathbf{M}_d^{-1}\mathbf{K}_d\Delta\mathbf{x} - \mathbf{M}_d^{-1}\Delta\mathbf{f} = \mathbf{0}, \quad (5)$$

where $\Delta\mathbf{x} = \mathbf{x} - \mathbf{x}_d$ and $\Delta\mathbf{f} = \mathbf{f}_e - \mathbf{f}_d$.

Next, by introducing the matrices $\boldsymbol{\Lambda}$, $\boldsymbol{\Gamma}$, and the vector $\Delta\mathbf{f}_l$ as [16]

$$\boldsymbol{\Lambda} + \boldsymbol{\Gamma} = \mathbf{M}_d^{-1}\mathbf{C}_d, \quad (6)$$

$$\boldsymbol{\Lambda}\boldsymbol{\Gamma} = \mathbf{M}_d^{-1}\mathbf{K}_d, \quad (7)$$

$$\Delta\dot{\mathbf{f}}_l + \boldsymbol{\Gamma}\Delta\mathbf{f}_l = \mathbf{M}_d^{-1}\Delta\mathbf{f}, \quad (8)$$

an impedance vector can be proposed as

$$\mathbf{z} = \Delta\dot{\mathbf{x}} + \boldsymbol{\Lambda}\Delta\mathbf{x} - \Delta\mathbf{f}_l, \quad (9)$$

such that the left side of (5) equals to

$$\Delta\ddot{\mathbf{x}} + \mathbf{M}_d^{-1}\mathbf{C}_d\Delta\dot{\mathbf{x}} + \mathbf{M}_d^{-1}\mathbf{K}_d\Delta\mathbf{x} - \mathbf{M}_d^{-1}\Delta\mathbf{f} = \dot{\mathbf{z}} + \boldsymbol{\Gamma}\mathbf{z}. \quad (10)$$

From (10), the impedance vector \mathbf{z} can be treated as the low-pass-filtered signal of the desired impedance model. In this paper, the control objective is formulated as $\mathbf{z} \rightarrow \mathbf{0}$ as $t \rightarrow \infty$, indicating the realization of the desired impedance model in the low-frequency range.

C. Structured-Light Technology

A collection of projected rays in the spatial direction is called structured light. The structured-light system is characterized by a set of projectors and cameras. The working principle of the structured-light system is shown in Fig. 2(a). The projector projects a specific patterned image onto the target object first, and the cameras capture the distorted image due to three-dimensionally shaped surface, then the processor processes the raw data from the camera and outputs the reconstructed position of the object. For the sake of avoiding obstructions, two cameras are usually installed to capture the image from different angles of view. The advantages of structured-light technology are listed as follows: firstly, since the structured light actively projects the coded light, it is very suitable for using in scenes with insufficient illumination (even no light) and lack of texture (such as sanded object in this paper). Secondly, the structured light projection pattern is specially designed to achieve high measurement accuracy within a certain range.

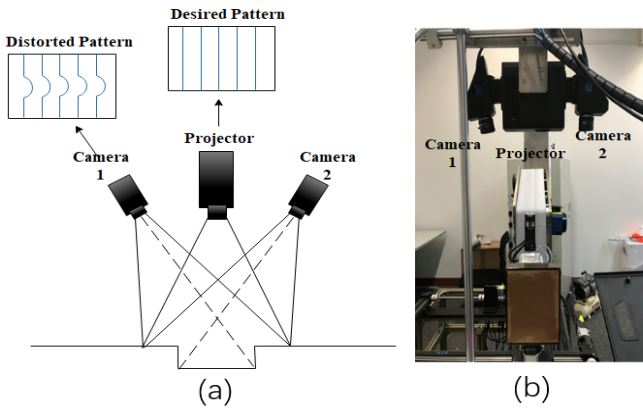


Fig. 2. (a) Working principle of a structured-light system; (b) A structured-light scanner.

A structured-light scanner is shown in Fig. 2(b). The scanned data is recorded in the form of dots, named point clouds, each of which contains three-dimensional coordinates, and some may contain color information (RGB) or reflection intensity information (intensity). The applications of the structured-light scanner include motion tracking [17], freeform surfaces inspection [18] and anthropometric parameter estimation [19] and so on. With advance of computer vision and electronic devices, structured-light scanner become more popular in industry robots.

III. AUTONOMOUS SANDING ROBOT

In this paper, a robotic system is developed to achieve the autonomous sanding with the work flow shown in Fig. 3. First, a structured-light scanner is used to scan the target object and reconstruct its CAD model with the point clouds. Second, a planning method is proposed to generate the sanding sequence for different surfaces of the object by referring to the CAD model. Third, an adaptive impedance controller is developed to drive the robot to perform the sanding task by following the optimized sequence. At the end of each sanding procedure, the sanded surface is automatically assessed by

employing the structured-light technology. If the sanding quality passes the assessment, the robot proceeds to sand the next surface or the next object. Otherwise, the same surface is sent back for re-sanding till its quality meets the requirement.

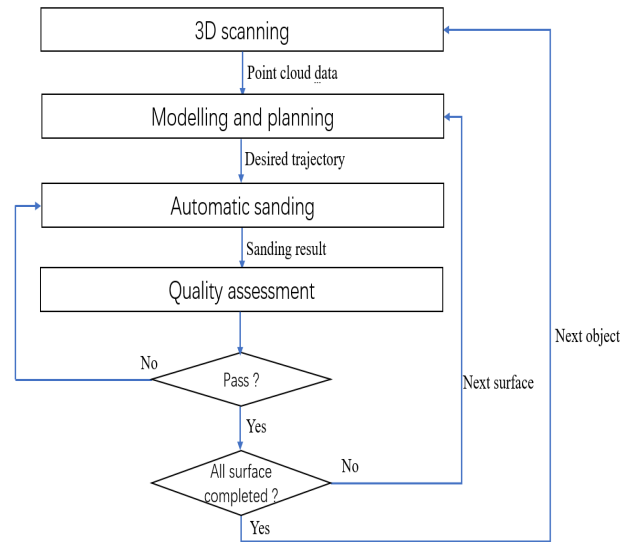


Fig. 3. Overall structure of the autonomous sanding robot

A. Mechanical Design

The mechanical structure of the sanding robot is shown in Fig. 4(a), consisting of the robot arm, the end effector, the mechanism of sanding belt, and the sensing and control module. To achieve the sanding task, the robot is controlled to grasp the object then manipulate it to physically interact with the sanding belt. The robotic arm has four degrees of freedom (DOFs), that is, two translational joints (to position the object) and two revolute joints (to adjust its orientation with respect to the sanding belt). The ATI force sensor is mounted on the robot arm shown in Fig. 4(b) to collect interaction force between backplate and sanded object during the operation. The control module consists of four servo motors to control the four joints shown in Fig. 4(b), IO module and frequency conversion device. IO module is implemented to send switching signals to pneumatic components and frequency conversion device is used to control the speed of sanding.

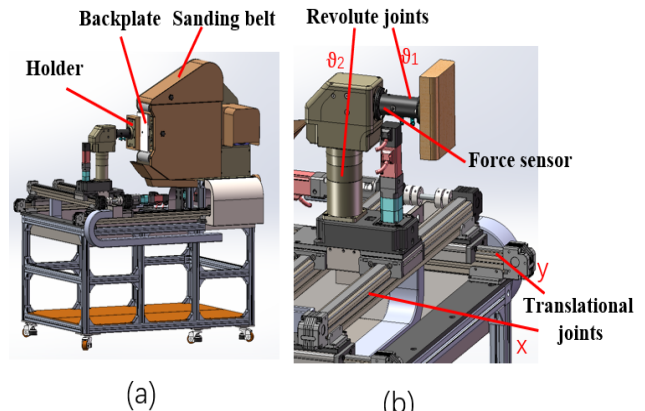


Fig. 4. The CAD model of the autonomous sanding robot (a) The overall structure; (b) The robot arm and the sanding end effector.

As seen in Fig. 4, an air cylinder push-pull mechanism is designed and installed on the end effector to grasp the sanded object. In particular, the piston of the cylinder can push a linkage mechanism that drives the four rubber fingers simultaneously to grasp the object. When the robotic arm comes back to the docking position, the piston pulls the linkage mechanism reversely and hence the grasping is released. An adjustable mechanism is also designed for the back plate which is used to make sure the backplate is perpendicular to the ground. The backplate and holder are controlled by pneumatic drivers. The back plate can make sure that the object and the sanding belt contact tightly with each other. Note that such design in Fig. 4 is general and can be easily extended to many different sanded objects. Because i) it has four DOFs which is sufficient for the sanding of objects with regular shapes, and ii) the end effector can be customized and replaced to suit the specific size and shape of objects.

B. Modeling and Planning

The proposed robot is able to sand the object without knowing the CAD model beforehand. The unknown object is scanned by the structured-light scanner first, then its CAD model is constructed with the point clouds generated by the scanner. In particular, the modeling consists of three steps (see Fig. 5). First, the field limits filter is set up to ensure the data captured are all from the sanded object but not from the sanding robot holder. Second, the Statistical Outlier Removal(SOR) filter [20] is applied to remove outliers in the collected data. Third, the 3D registration method [21-23] is employed to retrieve the whole structure of the sanded object.

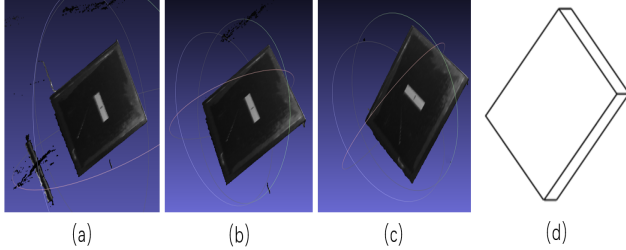


Fig. 5. Modeling with the structured-light scanner (a) Raw data; (b) After the processing with the field limits filter; (c) After the processing with the SOR Filter; (d) CAD model

The basic idea in registration is to convert every data in different coordinate systems into one unified coordinate system and minimize the error, that is, $\min\{\sum_{i=1}^k \|\mathbf{y}_{ai} - \mathbf{R}(\mathbf{y}_{oi}) - \mathbf{T}\|^2\}$, where \mathbf{R} denotes the rotation matrix, \mathbf{T} denotes the translation vector, \mathbf{y}_{oi} and \mathbf{y}_{ai} represent the points under the original coordinate system and the points under aimed coordinate system respectively. The mapping between two points is represented as $\mathbf{y}_{ai} = \mathbf{R}(\mathbf{y}_{oi}) + \mathbf{T}$. Therefore, given k pairs of matching points, it is to seek the rotation matrix \mathbf{R} and translation vector \mathbf{T} to minimize the error. In this paper, in order to scan different faces of the target object, the object is manipulated to rotate around θ_2 (see Fig. 4(b)) then the rotation matrix \mathbf{R} and the translation

vector \mathbf{T} are computed with the algorithm of Iterative Closest Point (ICP) [22] under such configuration.

With the constructed CAD model, the model-based planner is proposed to generate the desired trajectory for the robot. The planner is designed with the hierarchical structure. In the upper level, the multi-query method is used to optimize the sanding sequence for all the surfaces of the object. In the lower level, the single-query method is used to optimize the motion of the robot from one configuration to another.

In the single-query method, the objective is to generate the collision-free path with the desired speed and the acceleration. To obtain the collision-free path, consider the vertices of polyhedrons which enclose target object and platform CAD model: $\mathbf{V}_o = \{v_{o1}, v_{o2} \dots\}$, $\mathbf{V}_p = \{v_{p1}, v_{p2} \dots\}$, with their corresponding connect sequence: $\mathcal{S}_o, \mathcal{S}_p$, and initial and goal configurations of the robot: $\mathbf{q}_{start}, \mathbf{q}_{goal}$. Then, the collision-free path of the robot is generated as

$$\mathbf{c} = F_p(\mathbf{V}_o, \mathbf{V}_p, \mathcal{S}_o, \mathcal{S}_p, \mathbf{q}_{start}, \mathbf{q}_{goal}), \quad (11)$$

where $\mathbf{c}: [0, m] \rightarrow \mathcal{Q}$, $\mathbf{c}(0) = \mathbf{q}_{start}$, $\mathbf{c}(m) = \mathbf{q}_{goal}$, $\mathbf{c}(s) \in \mathcal{Q}_{free}$, $\forall s \in [0, m]$, F_p denotes the process of path planning, \mathcal{Q} denotes the configuration space, \mathcal{Q}_{free} denotes the configuration space which ensures collision-free criterion, s is the time step, and m is the length of time steps. The main idea of the method (11) is to connect the initial configuration and the goal configuration with a straight line then check if it is a collision-free path. The path of the robot should be updated if there exists a collision. In this paper, the collision checking is based on GJK algorithm, which iteratively generates simplex to determine whether the Minkowski difference of two convex shape includes the origin, and many algorithms are developed to deal with collision avoidance, for complicated environment, Probabilistic Road Map (PRM), Rapidly-Exploring Random Tree(RRT) can be adopted, while for simple obstacles, specific rules can be set to guide the robot away from obstacles [24]. After the collision-free motion is obtained, the method of Linear Segment with Parabolic Blend(LSPB) [25] is used to further shape it to achieve the desired speed and the desired acceleration such that the speed of motor can be maintained in its maximum level for a certain duration (that is, with higher efficiency).

In the multi-query method, the summation of weighted squared displacement is set as the objective function, as shown in (12), where \mathbf{w} is the weight vector to rescale the rotational distance and translational distance, h the index of sub-objective. Then, the Genetic algorithm is employed to obtain the sanding sequence with the minimum travel distance.

$$F_{cost} = \sum_h \sum_s \|\mathbf{w}(\mathbf{c}_h(s+1) - \mathbf{c}_h(s))\|^2, \quad (12)$$

C. Adaptive Impedance Control

The control objective of the sanding robot is to realize the desired impedance model (4) and hence carry out the sanding task on the target surface. First, a new impedance vector is formulated in joint space as

$$\mathbf{z}_q = \dot{\mathbf{q}} - \dot{\mathbf{q}}_r = \dot{\mathbf{q}} - \mathbf{J}^+(\mathbf{q})(\dot{\mathbf{x}}_d - \Lambda \Delta \mathbf{x} + \Delta \mathbf{f}_l), \quad (13)$$

where $\mathbf{J}^+(\mathbf{q})$ is the pseudo-inverse matrix, and

$$\dot{\mathbf{q}}_r = \mathbf{J}^+(\mathbf{q})(\dot{\mathbf{x}}_d - \mathbf{\Lambda}\Delta\mathbf{x} + \Delta\mathbf{f}_l), \quad (14)$$

is a reference vector.

From (9) and (13), it can be obtained that

$$\mathbf{z} = \mathbf{J}(\mathbf{q})\mathbf{z}_q. \quad (15)$$

Hence, the convergence of $\mathbf{z}_q \rightarrow \mathbf{0}$ implies that $\mathbf{z} \rightarrow \mathbf{0}$, that is, the realization of the desired impedance model.

Using (13), the dynamic model (3) can be written as

$$\begin{aligned} \mathbf{M}(\mathbf{q})\ddot{\mathbf{q}}_q + \mathbf{C}(\mathbf{q}, \dot{\mathbf{q}})\dot{\mathbf{z}}_q + \mathbf{M}(\mathbf{q})\ddot{\mathbf{q}}_r + \mathbf{C}(\mathbf{q}, \dot{\mathbf{q}})\dot{\mathbf{q}}_r + \mathbf{g}(\mathbf{q}) \\ = \boldsymbol{\tau}_e + \mathbf{u}. \end{aligned} \quad (16)$$

In this paper, it is assumed that the dynamic parameters $\mathbf{M}(\cdot)$, $\mathbf{C}(\cdot)$, and $\mathbf{g}(\cdot)$ are unknown. Then, the term $\mathbf{M}(\mathbf{q})\ddot{\mathbf{q}}_r + \mathbf{C}(\mathbf{q}, \dot{\mathbf{q}})\dot{\mathbf{q}}_r + \mathbf{g}(\mathbf{q})$ is approximated with the adaptive neural networks (NNs) techniques [26][27]. The implementation of the adaptive NNs eliminates the phase of offline training, and it also eliminates the requirement of the exact structure of disturbances or robot dynamics. In particular, the radial-based-function (RBF) [28], NNs is employed in this paper as

$$\mathbf{M}(\mathbf{q})\ddot{\mathbf{q}}_r + \mathbf{C}(\mathbf{q}, \dot{\mathbf{q}})\dot{\mathbf{q}}_r + \mathbf{g}(\mathbf{q}) = \mathbf{W}\boldsymbol{\theta}(\mathbf{q}, \dot{\mathbf{q}}, \ddot{\mathbf{q}}_r) + \mathbf{E}, \quad (17)$$

where \mathbf{W} is the ideal weight matrix, $\boldsymbol{\theta}(\cdot)$ is the activation function, and \mathbf{E} is the vector of approximation error.

Next, the adaptive impedance controller is proposed as

$$\mathbf{u} = -\mathbf{K}_z\mathbf{z}_q + \hat{\mathbf{W}}\boldsymbol{\theta}(\mathbf{q}, \dot{\mathbf{q}}, \ddot{\mathbf{q}}_r) - k_g\mathbf{s}\mathbf{gn}(\mathbf{z}_q) - \boldsymbol{\tau}_e, \quad (18)$$

where $\mathbf{K}_z \in \mathfrak{R}^{n \times n}$ is a diagonal and positive-definite matrix, k_g is a positive constant, $\mathbf{s}\mathbf{gn}(\cdot)$ is a sign function, and $\hat{\mathbf{W}}$ is the estimate of \mathbf{W} , which is updated by

$$\dot{\hat{\mathbf{W}}}_j^T = -\mathbf{L}_j\boldsymbol{\theta}(\mathbf{q}, \dot{\mathbf{q}}, \ddot{\mathbf{q}}_r)z_{qj}, \quad (19)$$

where $\hat{\mathbf{W}}_j$ represents the j^{th} row vector of $\hat{\mathbf{W}}$, z_{qj} is the j^{th} element of \mathbf{z}_q , and \mathbf{L}_j are diagonal positive definite matrices.

Substituting (18) into (16) and using (17) yields

$$\begin{aligned} \mathbf{M}(\mathbf{q})\dot{\mathbf{z}}_q + \mathbf{C}(\mathbf{q}, \dot{\mathbf{q}})\mathbf{z}_q + \mathbf{K}_z\mathbf{z}_q + k_g\mathbf{s}\mathbf{gn}(\mathbf{z}_q) \\ + \Delta\mathbf{W}\boldsymbol{\theta}(\mathbf{q}, \dot{\mathbf{q}}, \ddot{\mathbf{q}}_r) + \mathbf{E} = \mathbf{0}, \end{aligned} \quad (20)$$

where $\Delta\mathbf{W} = \mathbf{W} - \hat{\mathbf{W}}$

Next, we have the following theorem to state the stability of the closed-loop system.

Theorem: *The adaptive impedance control scheme described by (18) and (19) ensures the convergence of the impedance vector to zero, that is, $\mathbf{z}_q \rightarrow \mathbf{0}$ as $t \rightarrow \infty$, if the control parameter k_g is chosen sufficiently large such that the following condition is satisfied*

$$k_g > b_u, \quad (21)$$

where b_u denotes the upper bound of \mathbf{E} .

Proof: First, a Lyapunov-like candidate is defined as:

$$V = \frac{1}{2}\mathbf{z}_q^T\mathbf{M}(\mathbf{q})\mathbf{z}_q + \frac{1}{2}\sum_{j=1}^n\Delta\mathbf{W}_j\mathbf{L}_j^{-1}\Delta\mathbf{W}_j^T. \quad (22)$$

Next, differentiating V with respect to time, we have:

$$\dot{V} = \mathbf{z}_q^T\mathbf{M}(\mathbf{q})\dot{\mathbf{z}}_q + \frac{1}{2}\mathbf{z}_q^T\dot{\mathbf{M}}(\mathbf{q})\mathbf{z}_q - \sum_{j=1}^n\dot{\hat{\mathbf{W}}}_j\mathbf{L}_j^{-1}\Delta\mathbf{W}_j^T. \quad (23)$$

Substituting the closed-loop equation (20), new impedance vector (13) and the update law (19) into (23) and using Property (iii), we have:

$$\begin{aligned} \dot{V} = -\mathbf{z}_q^T\mathbf{K}_z\mathbf{z}_q - \mathbf{z}_q^T\{k_g\mathbf{s}\mathbf{gn}(\mathbf{z}_q) + \Delta\mathbf{W}\boldsymbol{\theta}(\mathbf{q}, \dot{\mathbf{q}}, \ddot{\mathbf{q}}_r) + \mathbf{E}\} \\ - \sum_{j=1}^n\dot{\hat{\mathbf{W}}}_j\mathbf{L}_j^{-1}\Delta\mathbf{W}_j^T = -\mathbf{z}_q^T\mathbf{K}_z\mathbf{z}_q - \mathbf{z}_q^T\mathbf{E} - k_g\mathbf{z}_q^T\mathbf{s}\mathbf{gn}(\mathbf{z}_q). \end{aligned} \quad (24)$$

Note that $-\mathbf{z}_q^T\mathbf{E} - k_g\mathbf{z}_q^T\mathbf{s}\mathbf{gn}(\mathbf{z}_q) \leq -(k_g - b_u)\|\mathbf{z}_q\|$. Therefore, if the condition (21) is satisfied, we have

$$\dot{V} \leq -\mathbf{z}_q^T\mathbf{K}_z\mathbf{z}_q \leq 0. \quad (25)$$

Hence, we have $V > 0$ and $\dot{V} \leq 0$. Therefore, V is bounded. The boundedness of V ensures the boundedness of \mathbf{z}_q and $\Delta\boldsymbol{\theta}$. The boundedness of \mathbf{z}_q ensures the boundedness of \mathbf{z} (see (15)). The boundedness of \mathbf{z} ensures the boundedness of $\Delta\dot{\mathbf{x}}$ and $\Delta\mathbf{x}$ from (9). From (14), since $\dot{\mathbf{x}}_d$, $\Delta\mathbf{x}$, and $\Delta\mathbf{f}_l$ are bounded, $\dot{\mathbf{q}}_r$ is bounded. Since both \mathbf{z}_q and $\dot{\mathbf{q}}_r$ are bounded, $\dot{\mathbf{q}} = \mathbf{z}_q + \dot{\mathbf{q}}_r$ is bounded. Differentiating (14) with respect to time, it is also concluded that $\ddot{\mathbf{q}}_r$ is bounded. Since $\ddot{\mathbf{q}}_r$, $\dot{\mathbf{q}}_r$, $\Delta\mathbf{W}$, and \mathbf{z}_q are all bounded, $\dot{\mathbf{z}}_q$ is bounded from (20). Therefore, \mathbf{z}_q is uniformly continuous. From (25), \mathbf{z}_q is bounded in L^2 . Then it follows [29] that $\mathbf{z}_q \rightarrow \mathbf{0}$. Hence, the desired impedance model is achieved. ■

IV. EXPERIMENT

The experiment equipment has been set up in The Chinese University of Hong Kong. The whole equipment is shown in Fig. 6. All the joints are driven by AC servo motors which are controlled by IMC30G-E-032PCI control board. In this experiment, the sanded object is a thirteen faces wooden box shown in Fig. 7. Control system is used to control the four translational and rotational joints noted as x , y , θ_1 , θ_2 (shown in Fig. 4(b)) and the sanding belt. The visual detecting system includes a 3D scanner, computer with 1080Ti and user interface to collect the original point clouds of the wooden box before and after sanding.

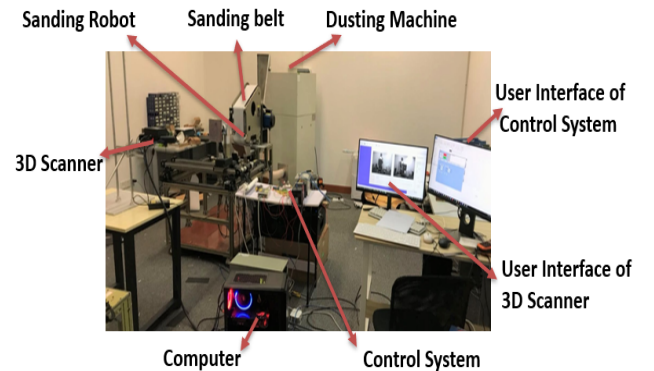


Fig. 6. Overall structure of experient setup

Before the experiment, adjust the back plate adjustment tool to parallel compliance with the surface on the top of the box and tune the frequency conversion device to make

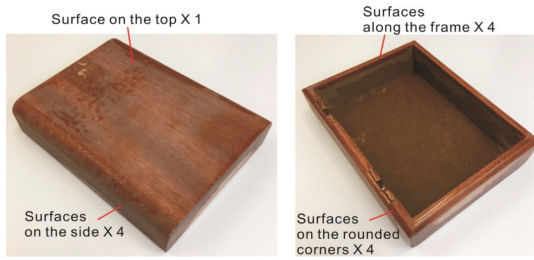


Fig. 7. Sanded object with 13 faces

the sanding belt moving under a proper speed. When the experiment begins, firstly, the wooden box is scanned by the structured-light camera and then the computer generates the accurate structure of the sanded object after processing. Then the autonomous sanding goes to the motion planning procedure, take one task in single-query method for example, the goal is to change the target surface from one surface on the side to its neighboring surface on the rounded corner. Directly connect initial and goal configurations returns collided path, so the path is updated, and then the desired speed and acceleration are given by LSPB. The results of trajectories of four joints are shown in Fig.8.

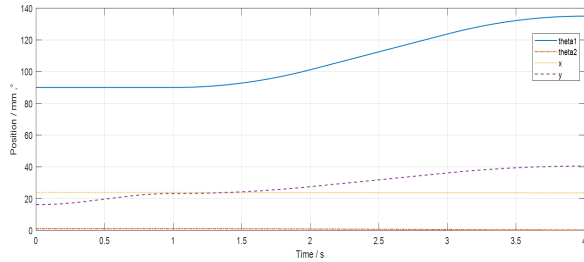


Fig. 8. Single-Query method

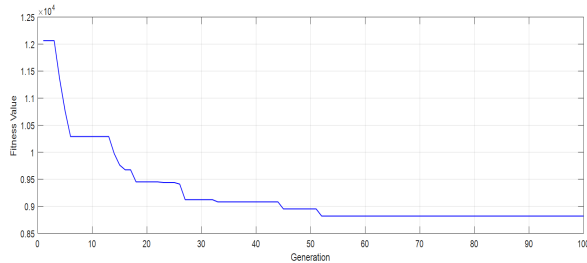


Fig. 9. Sanding Sequence Optimization

The motion planner uses Genetic Algorithm(GA) to optimize the task sequence in the multi-query method. Set population size as 200, crossover probability as 0.9, mutation probability as 0.1, maximum generation as 100, the optimization result is shown in Fig.9.

When the sanded object contact with the sanding belt, the back plate will pop out to make sure the tight contact and then sanding the object with adaptive impedance controller in the sanding direction, the desired contact force during sanding f_d is $-25N$, desired position x_d is 51.5mm. Control parameters $\Lambda = 11.5$, $\Gamma = 1$, $K_z = 10$, $k_g = 20$ and according to (6-8) the desired impedance model was set as $M_d = 1$, $C_d = 12.5$, $K_d = 11.5$, The impedance error z_q and control input torque u are shown in Fig. 11.

The box after sanding goes back to the vision detection position to evaluate the quality of sanding. The point clouds

before and after sanding could be seen in Fig. 10(a) and Fig. 10(b). We can see that the difference in terms of the number of overexposure points between these two point clouds.

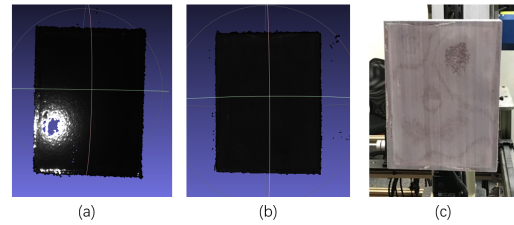


Fig. 10. (a) Point cloud data before sanding procedure (b) Point cloud data after sanding procedure (c) The box after sanding

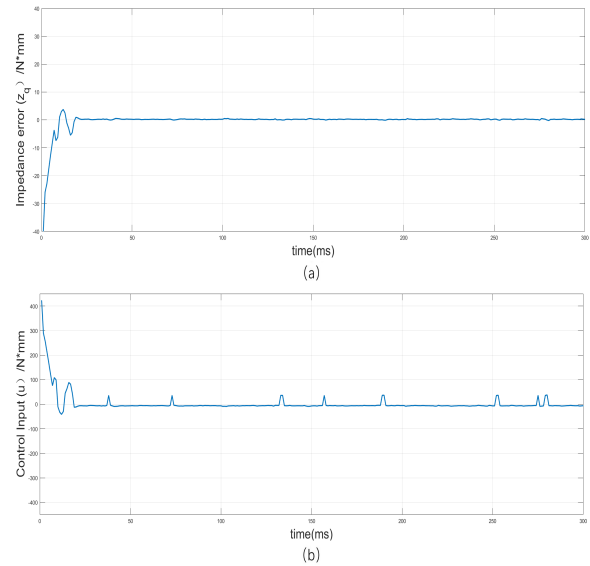


Fig. 11. (a) Impedance error (b) Control input

In the manufacturing of the wooden box, because of the uneven force and vibration produced during the procedure, it is hard to even skilled workers to sand out the last 0.2mm on the box. However, for this autonomous sanding robot with the structured-light scanner, it is easy to control the force and position of the box without the accurate dynamic model given beforehand. The result of the box after sanding show in Fig. 10(c).

V. CONCLUSION

In this paper, a new sanding robot has been developed to automate the labor-intensive works. The structured-light technology has been employed to scan the unknown object and hence obtain its CAD model online. The model-based planning method has been presented to optimize the motion of the robot end effector. The adaptive impedance controller has been proposed to drive the robot to carry out the sanding task. The stability of the closed-loop system is rigorously proved using Lyapunov methods, with the consideration of uncertain dynamic parameters. The developed robot has the advantage of highly autonomous capability, in the sense that no human assistance or involvement is required in any steps of the whole procedure of sanding. The performance of the robot has been validated in the sanding experiments on a batch of wooden boxes.

REFERENCES

- [1] Nagata, Fusaomi and Watanabe, Kimitsuna and Izumi, Kiyotaka. (2001). Furniture polishing robot using a trajectory generator based on cutter location data. Proceedings - IEEE International Conference on Robotics and Automation. 1. 319 - 324 vol.1. 10.1109/ROBOT.2001.1620978.
- [2] Nagata, Kusumoto, Watanabe, Kiguchi, Tsuda, Yasuda, Yokoyama, Umetsu, Mori, and Omoto. "High Precision Polishing Robot Using a Learning-based Surface following Controller." Computational Intelligence in Robotics and Automation, 2003. Proceedings. 2003 IEEE International Symposium on 1 (2003): 91-96.
- [3] Tsai, Jou-Lung Chang, and Jian-Feng Haung. "Development of an Automatic Mold Polishing System." Automation Science and Engineering, IEEE Transactions on 2, no. 4 (2005): 393-97.
- [4] Nagata, Kusumoto, Fujimoto, and Watanabe. "Robotic Sanding System for New Designed Furniture with Free-formed Surface." Robotics and Computer Integrated Manufacturing 23, no. 4 (2007): 371-79.
- [5] Eriksen, Arentoft, Grnbk, and Bay. "Manufacture of Functional Surfaces through Combined Application of Tool Manufacturing Processes and Robot Assisted Polishing." CIRP Annals - Manufacturing Technology 61, no. 1 (2012): 563-66.
- [6] T. M. Stephen, L. M. Sweet, M. C. Good, and M. Tomizuka, "Control of tool workpiece contact force with application to robotic deburring," IEEE J. Robotics Autom., vol. 3, no. 1, pp. 7-18, 1987.
- [7] H. Kazerooni, "Robotic deburring of two-dimensional parts with unknown geometry," J. Manuf. Syst., vol. 7, no. 4, pp. 329-338, 1988.
- [8] Oba, and Kakinuma. "Simultaneous Tool Posture and Polishing Force Control of Unknown Curved Surface Using Serial-parallel Mechanism Polishing Machine." Precision Engineering 49 (2017): 24-32.
- [9] Mohammad, Hong, and Wang. "Design of a Force-controlled End-effector with Low-inertia Effect for Robotic Polishing Using Macro-mini Robot Approach." Robotics and Computer Integrated Manufacturing 49 (2018): 54-65.
- [10] Tian, Lv, Li, and Liu. "Modeling and Control of Robotic Automatic Polishing for Curved Surfaces." CIRP Journal of Manufacturing Science and Technology 14 (2016): 55-64.
- [11] M. H. Raibert and J. J. Craig, "Hybrid position/force control of manipulators," J. Dyn. Syst., Meas., Control, vol. 103, no. 2, pp. 126-133, 1981.
- [12] N. Hogan, "Impedance control-An approach to manipulation. I-Theory.II-Implementation. III-Applications," J. Dyn. Syst., Meas., Control, vol. 107, pp. 1-24, Mar. 1985.
- [13] Li, Xiang, Yongping Pan, Gong Chen, and Haoyong Yu. "Adaptive Human-Robot Interaction Control for Robots Driven by Series Elastic Actuators." Robotics, IEEE Transactions on 33, no. 1 (2017): 169-82.
- [14] Sheng, and Zhang. "Fuzzy Adaptive Hybrid Impedance Control for Mirror Milling System." Mechatronics 53 (2018): 20-27.
- [15] C. C. Cheah and X. Li, Task-Space Sensory Feedback Control of Robot Manipulator, Springer, 2015.
- [16] Li, Liu, and Yu. "Iterative Learning Impedance Control for Rehabilitation Robots Driven by Series Elastic Actuators." Automatica 90 (2018): 1-7.
- [17] Erikshj, Olesen, Conradsen, Hjgaard, and Larsen. "Structured Light-based Motion Tracking in the Limited View of an MR Head Coil." Nuclear Inst. and Methods in Physics Research, A 702 (2013): 117-20.
- [18] Wu, Qian, Wei Zou, and De Xu. "Viewpoint Planning for Freeform Surface Inspection Using Plane Structured Light Scanners." International Journal of Automation and Computing 13, no. 1 (2016): 42-52.
- [19] Stancic, Music, and Zanchi. "Improved Structured Light 3D Scanner with Application to Anthropometric Parameter Estimation." Measurement 46, no. 1 (2013): 716-26.
- [20] Balta, Velagic, Bosschaerts, De Cubber, and Siciliano. "Fast Statistical Outlier Removal Based Method for Large 3D Point Clouds of Outdoor Environments." IFAC PapersOnLine 51, no. 22 (2018): 348-53.
- [21] Besl, P.J., and Neil D. McKay. "A Method for Registration of 3-D Shapes." Pattern Analysis and Machine Intelligence, IEEE Transactions on 14, no. 2 (1992): 239-56.
- [22] Rusinkiewicz, S., and M. Levoy. "Efficient Variants of the ICP Algorithm." 3-D Digital Imaging and Modeling, 2001. Proceedings. Third International Conference on, 2001, 145-52.
- [23] Forsyth, David., and Jean. Ponce. Computer Vision : A Modern Approach. 2nd ed. Boston: Pearson, 2012.
- [24] Choset H, Lynch K and Hutchinson S. "Principles of Robot Motion:Theory, Algorithms, and Implementations". The MIT Press, 2005.
- [25] Corke P. Robotics, "Vision and Control: Fundamental Algorithms in MATLAB". Springer, 2011.
- [26] Xiang Li, and Chien Chern Cheah. "Adaptive Neural Network Control of Robot Based on a Unified Objective Bound." IEEE Transactions on Control Systems Technology 22, no. 3 (2014): 1032-043.
- [27] Liangyong Wang, Tianyou Chai, and Chunyu Yang. "Neural-Network-Based Contouring Control for Robotic Manipulators in Operational Space." IEEE Transactions on Control Systems Technology 20, no. 4 (2012): 1073-080.
- [28] Biancolini, Marco Evangelos. Fast Radial Basis Functions for Engineering Applications, 2017.
- [29] Slotine, J.-J. E., and Weiping. Li. Applied Nonlinear Control. Englewood Cliffs, N.J.: Prentice Hall, 1991.